Electronic Supplementary Material (ESI) for Journal of Materials Chemistry A.
This journal is © The Royal Society of Chemistry 2022
Please do not adjust margins

ARTICLE

Controllable Interfacial Electron Transfer Induced by Heterointerfaced Sulfur-based Catalysts with Lower Electronegative Anion for Boosted Hydrogen Evolution Reaction in Universal pH Range

Received 00th January 20xx,
Accepted 00th January 20xx

DOI: 10.1039/x0xx00000x

Dawei Chu [a, b, ‡], Xiaoling Wei [c, ‡], Xiumei Song [d, f ‡], Zhen Zhang [e], Lichao Tan [a, f *], Huiyuan Ma [a, *], Haijun Pang [a], Xin Wang [c, f], and Zhongwei Chen [e, *]

Economic cobalt-sulfide (Co_xS_y)-based electrocatalysts play a vital role in the hydrogen evolution reaction (HER) due to its adjustable electronic structure and environmental friendliness. However, the limited active sites, poor structural stability and intense hydrogen (H) adsorption energy of these catalysts endow themselves with unsatisfied performance, which significantly impede their practical application in acidic/alkaline/neutral media. Herein, we designed a series of defective nickel-cobalt sulfur-based catalysts with enriched heterogeneous interface. The P anions not only offers ample sulfur defects for charge movement, but also provides a protection layer to avoid structural collapse in acidic/alkaline media. More importantly, the P elements with low electronegative slightly lower the robust strength of S-H bonds, yet maintain the activity of the S-based catalysts, thereby balancing the adsorption/release of H. Subsequently, the introduction of heterointerface accompanied by P creates the controllable interfacial electron transfer between Ni-based components ($Ni_3S_xP_y$) and Co components ($Co_3S_xP_y$), which can regulate the charge state and enhance charge transfer kinetics for boosted HER. Meanwhile, the planar structure establishes high conductive network for facilitated ion/electron transportation, conferring accelerated redox reaction. Attributed to its structural benefits, an admirable HER performance with the optimum overpotential of 56 mV and Tafel slope of 74 mV dec^{-1} with -10 mA cm^{-2} in 1 M KOH and decent long-term stability can be achieved. This work paves the way for S-based catalysts design to achieve superior HER performance in universal pH range.

Introduction

Hydrogen (H_2) has been demonstrated as one of the most potential renewable energy resources. Electrocatalytic water splitting is a superior energy conversion and storage technology to generate H_2 compared to other methods.[1-5] Currently, Platinum (Pt)-based materials are considered as the most excellent electrocatalysts for hydrogen evolution reaction (HER) because of the superior conductivity and lowest Gibbs free energy. Nonetheless, their development is limited due to the high cost and content scarcity.[6-8] In particular, Pt-based materials are unable to obtain superb electrocatalytic performance for HER in a universal pH range.[9] As such, it is essential to construct the efficient electrocatalysts with Pt-free in a wide pH range.

Recently, transition metal (Ni, Co, Fe and Cu) based materials have been widely considered as an alternative to Pt-based catalysts for HER owing to its cost-effectiveness and environmental benignity.[10-13] Among TMSs, cobalt sulfide (Co-S) possesses high catalytic activity and easy accessibility. However, the low conductivity, scarce active sites, unsteady structure and the excessive S-H bonds (H atoms adsorption on S sites) on the surface of cobalt sulfide detriments it's HER performance.[14-18]

Consequently, employing effective methods to tune their electrocatalytic performance for HER is extremely vital, such as doping introduction, single-atom decoration, heterogeneous interfaces and defect engineering.[11,19,20] Moreover, the heterointerface engineering have been introduced to realign electronic structure *via* interfacial electronic effect.[18-22] In addition, the heterointerfaced electrocatalysts can offer multiple active sites and enable fast electron transfer between different components, rendering favored HER process.[23,24] Ni-based materials can be considered as another heterogeneous interface for HER because of its high activity and conductivity,

[a.] *School of Materials Science and Chemical Engineering, Harbin University of Science and Technology, Harbin 150040, P. R. China. E-mail: lctan@hrbust.edu.cn; mahy017@nenu.edu.cn.*
[b.] *Department of Materials Science and Engineering, National University of Singapore, Singapore 117574, Singapore.*
[c.] *South China Academy of Advanced Optoelectronics & International Academy of Optoelectronics at Zhaoqing, South China Normal University, Guangdong 510006, China.*
[d.] *State Key Laboratory of Urban Water Resource and Environment, School of Environment, Harbin Institute of Technology, Harbin, 150090, P. R. China.*
[e.] *Department of Chemical Engineering, University of Waterloo, Waterloo, ON N2L 3G1, Canada. E-mail: zhwchen@uwaterloo.ca*
[f.] *Carbon Neutral Research Institute, Zhejiang Wanli University, Ningbo 315100, P.R. China*
†Electronic Supplementary Information (ESI) available: See DOI: 10.1039/x0xx00000x
‡ These authors contributed equally to this work.

Please do not adjust margins

Please do not adjust margins

which is critical to control the electronic structure of the Co-S interface. Besides, the introduction of P elements with lower electronegativity can enrich S defects while maintain the structural integrity, which can expose more specific crystal planes, offer more active sites and boost electron transfer, rendering improved conductivity and durability of entire cells. Hence, it is critical to design catalyst which synchronically incorporates heterostructure coupled with defect to enable the tunable binding abilities of hydroxyl ions (OH^*) and H^* for efficiently tailored water dissociation energy and boosted H^* conversion. However, design the catalyst with comparable performance to Pt-based catalysts based on these strategies still remains significant challenges.[5,25,26]

Herein, we propose to design the catalyst with controllable interfacial electronic transfer induced by heterointerface and lower electronegative P anions of defective nickel-cobalt sulfide sheets catalysts (V_S-NCSP-X/NF) for superior HER performance in universal pH range. The as-synthesized V_S-NCSP-10/NF samples present excellent electrocatalytic performance, such as the low overpotentials of 56 mV with -10 mA cm^{-2} and significant stability in 1 M KOH. These are attributed to the following points: (1) the interfacial electron transfer constructs an active electric field, providing favored catalytic activity for HER; (2) the introduction of P anions on heterointerface optimizes the H adsorption energy of S-based catalysts, leading to favored H^* Gibbs free energy similar to Platinum (Pt)-based electrocatalysts; (3) additionally, the ample sulfur defects not only effectively expedite electron transfer, but also offer abundant active sites, rendering accelerated reaction kinetics; (4) the P elements act as a protector that provide the anti-corrosion layer to prevent the damage of materials in acidic/alkaline media; (5) the structure uniqueness of V_S-NCSP-X/NF endows the electrocatalyst with high specific surface area and enriched active sites, laying the foundation for tailoring the HER process. Besides, density functional theory (DFT) calculations reveal that the H adsorption on Co sites is intensely stimulated by interfacial electronic. Moreover, differential charge density verifies the targeted movement of electrons attributed to the formation of heterogeneous interfaces while the materials possess a remarkably low Gibbs free energy near 0 eV due to synergistic effects of heterogeneous interfaces formation and P elements introduction. This work reports a deep insight into obtaining all-around catalysts for HER in a wide pH range.

Results and discussion

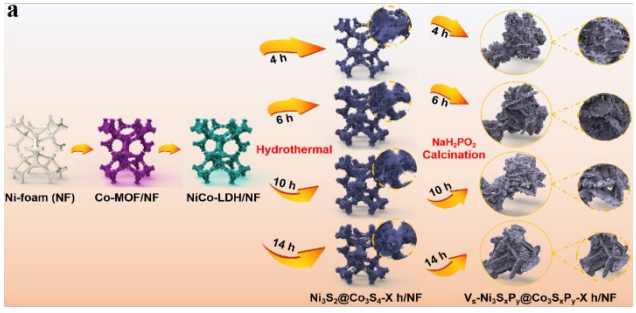

Fig. 1. (a) Schematic illustration of the synthesis of V_S-NCSP-X/NF.

The concise dipping and hydrothermal preparation processes of catalyst are elucidated in Fig. 1a. Three-dimensional prismatic cone-like ZIF-67 is firstly deposited on Ni-foam (NF) in the air for 4 h through the dipping method (Co-MOF/NF), illustrated in Fig. S1a. Afterward, the double-layered Ni-Co hydroxide (NiCo-LDH) is anchored on NF via the cation exchange method (NCL/NF). Unlike the Co-MOF/NF, the NCL/NF generates large amounts of wrinkles in the original smooth surface, validated by scanning electron microscopy (SEM) (Fig. S1b). To obtain NiCo-based sulfides, the NCL/NF is placed in an autoclave at 160 °C for a series of sulfurization reaction times (ST) (from 4 h to 14 h), which is denoted as the NCS-X/NF (Fig. S1c). Finally, the V_S-NCSP-X/NF is obtained by thermally annealing with $NaH_2PO_2 \cdot H_2O$ at 300 °C for 2 h (Fig. S1d). It is noted that the V_S-NCSP-X/NF samples appear more epitaxial sides based on the NCS-X/NF cross-linked sheets.

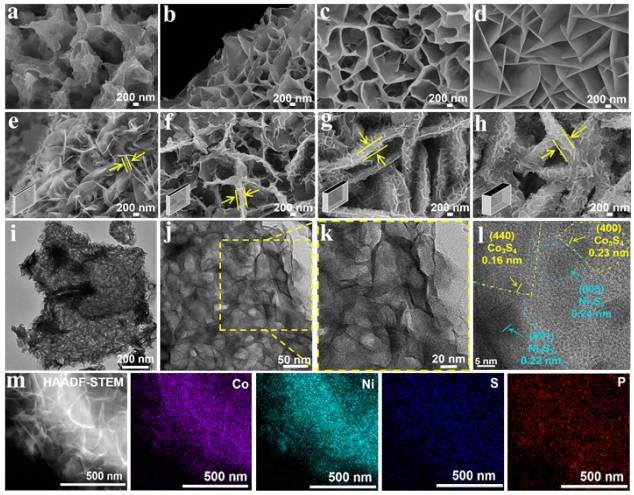

Fig. 2. SEM images of (a) NCS-4/NF; (b) NCS-6/NF; (c) NCS-10/NF; (d) NCS-14/NF; (e) V_S-NCSP-4/NF; (f) V_S-NCSP-6/NF; (g) V_S-NCSP-10/NF; (h) V_S-NCSP-14/NF; (Inset of images denoted as thickness of sheets' model). (i-k) TEM images of V_S-NCSP-10/NF. (l) HRTEM image of V_S-NCSP-10/NF. (m) HAADF and EDX elemental mappings images of V_S-NCSP-10/NF.

Presumably, these differences in ST may contribute to various shaped samples. Thereby, the structure of NCS-X/NF and V_S-NCSP-X/NF is more precisely elucidated by SEM (Fig. 2a-h). The cross-linked NCS-X sheets grow sharper and sharper with raising the ST from 4 h to 14 h (Fig. 2a-d). When the ratio of $M_{NCL/NF}$ to $M_{Thioacetamide}$ (M_{TAA}) is changed to 1 : 2 and 1 : 6, the samples become relative aggregation (Fig. S2a-b), yet this phenomenon is inversely proportional to the excellent electrochemical properties, which hinders the exposure of active sites. Subsequently, the introduction of the P anion drastically stimulates the increasement of epitaxial sides, leading to an enlarge specific surface area. In the case of overlong ST, the V_S-NCSP-X/NF samples get extremely thick, hindering the exposure of active sites. Also, the transmission electron microscopy (TEM) images validate that the V_S-NCSP-10/NF possesses several porous constructions and sides, as presented in Fig. 2i-k and Fig. S3a. Besides, the atomic force microscope (AFM) image of V_S-NCSP-10 (placed in Fig. S4) further demonstrates the sides on the sample surface. Furthermore, the high-resolution transmission electron

This journal is © The Royal Society of Chemistry 20xx

Please do not adjust margins

Please do not adjust margins

microscopy (HRTEM) image is engaged to detect the lattice fringes, heterogeneous interface and defects. Lattice spacings of 0.20 and 0.24 nm can be attributed to (021) and (003) facets of Ni_3S_2, while 0.16, 0.19, and 0.23 nm belong to (102), (110) and (114) facets of Co_3S_4 (Fig. 2l).[1,15-17,23] Interestingly, the heterogeneous interface can distinctly identify between $Ni_3S_xP_y$ and $Co_3S_xP_y$. The blurred/broken lattice fringes (can be observed in Fig. S3b) reflect and confirm the existence of defects. The high angle annular dark-field (HAADF) images of V_s-NCSP-10 display the numerous sides on the surface, as consistent with the SEM and AFM. Energy-dispersive X-ray (EDX) elemental mappings affirm the homogeneous distribution of the Ni, Co, S and P elements. Based on the selected area electron diffraction (SAED) patterns (Fig. S3c), the bright spots can be corresponded to the crystal planes of $Co_3S_xP_y$ and $Ni_3S_xP_y$.

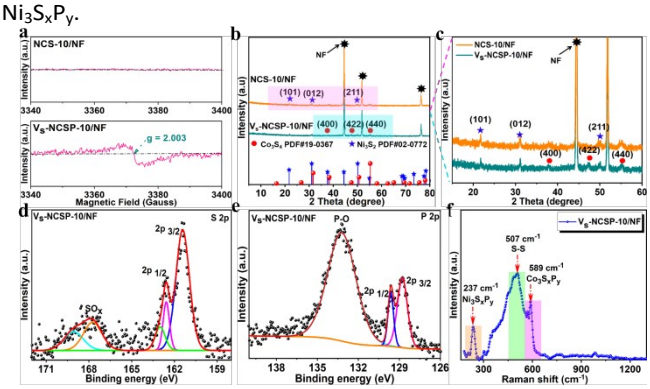

Fig. 3. (a) EPR spectra of NSC-10/NF and V_s-NCSP-10/NF. (b) XRD patterns of the catalysts. (c) An enlarged view of (b). XPS spectra of the catalysts: (d) S 2p; (e) P 2p. (f) Raman spectra of V_s-NCSP-10/NF.

To precisely demonstrate the appearance of S vacancies in the V_s-NCSP-10/NF, the electron paramagnetic resonance (EPR) characterization is carried out (depicted in Fig. 3a), a distinctive EPR signal can be detected at g = 2.003 for the catalyst, indicating that the introduction of P can induce the formation of defects, which are similar to marked defects image (Fig. S3b).[27-31] The diffraction peaks in the X-ray diffraction (XRD) pattern can be indexed to the Ni_3S_2 (JCPDS No. 02-0772) and Co_3S_4 (JCPDS No. 19-0367), respectively. Among diffraction peaks, (101), (012) and (211) planes belong to Ni_3S_2, and (400), (422) and (440) facets correspond to the Co_3S_4, indicating the presence of hetero-interface (Fig. 3b-c).[15-17,32]. Intriguingly, after phosphatization, all V_s-NCSP-X/NF samples exhibit relative peaks without other phosphides, confirming that the S sites are partially replaced with P (Fig. S5).[16,17] X-ray photoelectron spectroscopy (XPS) is employed to analyze the valence states. The survey of different samples verifies the presence of corresponding elements; Ni, Co, S and P elements of V_s-NCSP-10/NF, Ni, Co and S elements in NCS-10/NF and Co, S and P elements of V_s-CSP-10/NF (Fig. S6). Fig. S7 shows that the Ni 2p spectrum of V_s-NCSP-10/NF, which exhibits 0.5 eV positive shift more than NCS-10/NF due to the introduction of P atoms.[16] In the Co 2p spectrum of V_s-NCSP-10/NF (Fig. S8), two peaks correspond to the signals of Co $2p_{3/2}$ and Co $2p_{1/2}$ are related to 773.3 and 793.2 eV, respectively, corresponding with satellite peaks.[15-17,23,32,33] It is worth mentioning that compared to NCS-10/NF, the Co 2p peaks have an obvious shift, indicating the change in the electronic band bending that caused by interfacial interaction between $Ni_3S_xP_y$ and $Co_3S_xP_y$ along with P anion. the 161.4 and 162.6 eV peaks can be assigned to S $2p_{3/2}$ and S $2p_{1/2}$ in the S 2p spectrum (Fig. 3d), respectively.[15, 16, 33] And an inconspicuous sulfate feature is found in S 2p for V_s-NCSP-10/NF that the peak locates at 167.7 eV. A peak in the P 2p spectrum for V_s-NCSP-10/NF (Fig. 3e) is detected at 133.2 eV, belonging to the P-O bonds of phosphate species, which can be attributed to the surface of the oxidized phosphide by the air. Besides, the P 2p regions located at 128.7 and 129.6 eV can be ascribed to P $2p_{1/2}$ and P $2p_{3/2}$, respectively, suggesting the formation of Metal-P bonds.[21,33] The ratio of P/S atomic is counted to be approximately 3:1, originating from the XPS results of V_s-NCSP-X/NF and V_s-CSP-X/NF catalysts (Table S1). Moreover, Raman spectroscopy further characterizes the composition of the materials. The Raman spectrum of V_s-NCSP-10/NF shows that the S-S bond is at 507 cm^{-1}, confirming the forming of the Ni-S/Co-S phase. For V_s-NCSP-10/NF samples, many relatively weak peaks at 237 and 589 cm^{-1} are observed in Fig. 3f,[34-40] suggesting the satisfactory synthesis of $Ni_3S_xP_y$ and $Co_3S_xP_y$ species, respectively.

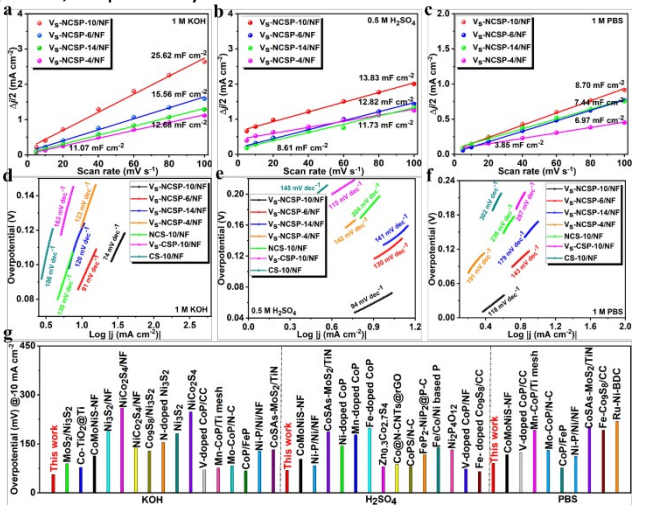

Fig. 4. Electrochemical double-layer capacitances (C_{dl}) of V_s-NCSP-X/NF samples in wide pH range: (a) 1 M KOH, (b) 0.5 M H_2SO_4, (c) 1 M PBS. The Tafel slopes of various catalysts for HER in (d) 1 M KOH, (e) 0.5 M H_2SO_4, (f) 1 M PBS. (g) Comparisons of HER overpotentials with other reported catalysts.

An effective electrocatalyst can work at all kinds of pH-universal electrolytes to meet the requirements of the HER procedure. Consequently, the HER properties of the prepared catalysts on NF as the working electrodes are inspected in 1 M KOH, 0.5 M H_2SO_4, and 1 M PBS, separately. Besides, the loading densities of all catalysts grown on NF are in the range of 1 mg/cm^2 - 2 mg/cm^2. The cyclic voltammetry (CV) curves demonstrate a stable position in different electrolytes at various scan rates from 5 mV s^{-1} to 100 mV s^{-1}, illustrated in Fig. S9-S11. Furthermore, the electrochemical surface area (ECSA) of V_s-NCSP-X/NF is dominated by the double-layer capacitance (C_{dl}) to explore accessible active sites and counted by CV characterization, as depicted in Fig. 4a-c. The C_{dl} values of V_s-NCSP-10/NF (1 M KOH: 25.62 mF cm^{-2}/0.5 M H_2SO_4: 13.83 mF cm^{-2}/1 M PBS: 8.70 mF cm^{-2}), V_s-NCSP-6/NF (1 M KOH: 15.56 mF

Please do not adjust margins

Please do not adjust margins

cm^{-2}/0.5 M H_2SO_4: 12.82 mF cm^{-2}/1 M PBS: 7.44 mF cm^{-2}), V_s-NCSP-14/NF (1 M KOH: 12.68 mF cm^{-2}/0.5 M H_2SO_4: 11.73 mF cm^{-2}/1 M PBS: 6.97 mF cm^{-2}) and V_s-NCSP-4/NF (1 M KOH: 11.07 mF cm^{-2}/0.5 M H_2SO_4: 8.61 mF cm^{-2}/1 M PBS: 3.85 mF cm^{-2}) prove that the V_s-NCSP-10/NF owns the maximum active sites regardless of the species of electrolyte solution. Hence, the position also verifies that this sample possesses a better structure than other catalysts, indicating the more active specific area/sites of V_s-NCSP-10/NF. The effect of P anion doping and heterostructure formation of all electrocatalysts are analyzed by the iR-corrected linear sweep voltammetry (LSV) curves and corresponding summary overpotentials in 1 M KOH, 0.5 M H_2SO_4 and 1 M PBS, as shown in Fig. S12-S13 and Table S2. Similar to ECSA results, the V_s-NCSP-10/NF shows excellent overpotentials of 56 mV (1 M KOH), 69 mV (0.5 M H_2SO_4) and 90 mV (1 M PBS) at -10 mA cm^{-2}, which are almost comparable to commercial Pt plate (1 M KOH: 20 mV; 0.5 M H_2SO_4: 30 mV; 1 M PBS: 56 mV). As proof, the NCS-10/NF samples obtain an inferior overpotential of 124 mV (1 M KOH), 207 mV (0.5 M H_2SO_4) and 214 mV (1 M PBS), suggesting that the limitation of sulfides in rough H adsorption energy slowdown the H_2 diffusion. Without the heterogeneous interface, the V_s-CSP provides a slow change transform, obtaining a trough HER performance (1 M KOH: 160 mV; 0.5 M H_2SO_4: 243 mV; 1 M PBS: 248 mV). Also, the NF substrate does not exhibit a significant donation for the HER performance (Fig. S12d-f). Besides, by comparing the HER overpotentials with other catalysts (shown in Fig. 4g and Table S3),[41-66] it can be observed that the reported catalyst is a strong competitor.

More importantly, the Tafel slope, one of the kinetic parameters, is investigated (displaying in Fig. 4d-f), and the Tafel slope of all samples is compared (Fig. S14 and Table S2). The electrochemical HER process possesses two reaction mechanisms in 1 M KOH, 1 M PBS and 0.5 M H_2SO_4. The reaction mechanisms are listed below:[8,10]

H^* adsorption process

1 M KOH/1 M PBS

$H_2O + e^- + {}^* \rightarrow OH^- + H^*$ Volmer step (1)

0.5 M H_2SO_4

$H_3O^+ + e^- + {}^* \rightarrow H_2O + H^*$ Volmer step (2)

H^* desorption process

1 M KOH/1 M PBS

$H^* + H_2O + e^- \rightarrow OH^- + H_2$ Heyrovsky step (3)

$H^* + H^* \rightarrow H_2$ Tafel step (4)

0.5 M H_2SO_4

$H^* + H_3O^+ + e^- \rightarrow 2\ H_2$ Heyrovsky step (5)

$H^* + H^* \rightarrow H_2$ Tafel step (6)

Based on the reaction mechanism, the V_s-NCSP-10/NF with heterointerface has a minimum Tafel slope except for the commercial Pt plate, which shows the HER process possibly determined by Volmer-Heyrovsky pathways. Compared with the commercial Pt plate, the other samples have a higher Tafel slope than 120 mV dec^{-1}, suggesting that their rate-determining step could be the Volmer step. The employment of heterointerface and P anion accelerate electrons transport and overcome the hindrance of excessive H adsorption energy by pure Volmer step, thereby accessing faster reaction kinetics.

Electrochemical impedance spectroscopy (EIS) is utilized to explore the kinetics of various electrolytes. The diameter of the semicircles is denoted as the charge transfer resistance (R_{ct}) within a high-frequency region and the behalf of the charge transfer resistance between the interface of electrode and electrolyte.[1,16] The R_{ct} of V_s-NCSP-10/NF is relatively similar to Pt plate with admirable conductivity in 1 M KOH, 0.5 M H_2SO_4 and 1 M PBS, further confirming the fast HER kinetics (Fig. S15). The stability performance is crucial to an excellent catalyst. Accordingly, the stability of V_s-NCSP-10/NF is tested based on the durable CV cycling and amperometric current density-time (I-t) curves measurement. As presented in Fig. S16, the LSV curves of V_s-NCSP-10/NF display no significant variation after 6000 circles compared with the initial state in different pH ranges. Moreover, the amperometric I-t curves characterization exhibits no evident recession after 12 h (shown in Fig. S17). Both CV cycling and I-t measurement demonstrate the delightful HER stability of V_s-NCSP-10/NF. For deep investigation, after electrochemical testing, the samples are characterized to inquiry robustness of the structure by SEM (Fig. S18), and no significant changes can be observed for each pH range, which corroborate the anti-corrosive effect of P elements. All above results verify that the V_s-NCSP-10/NF catalyst equipped with heterointerface and P anion possesses impeccable HER performance at all pH ranges.

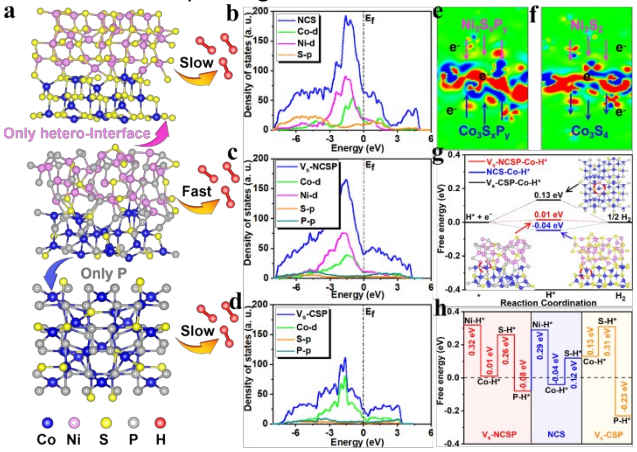

Fig. 5. (a) The optimized computational structure models of the different catalysts and schematic diagram of HER mechanism. Calculated density of states of (b) NCS; (c) V_s-NCSP; (d) V_s-CSP, the black line denotes as the position of the Fermi energy level. Differential charge density of (e) V_s-NCSP model and (f) NCS model. The red (blue) areas mark an increase (decrease) of the electron density. (g) Gibbs free energy (ΔG_{H^*}) on Co sites of V_s-NCSP, NCS and V_s-CSP. (h) the survey of Gibbs free energy (ΔG_{H^*}) on different sites of samples.

To understand the effect of heterointerface and P anion on catalytic properties in a wide PH range, the DFT calculations are implemented with the rationally atomic models based on the experimental characterization. Fig. 5a shows the optimized computational structure models and the HER mechanism, which indicate that the V_s-NCSP samples have better HER kinetics than NCS and V_s-CSP, similar to the experimental results. The density of states (DOS) (Fig. 5b-d, Fig. S19) data show that the Co d-band in Fermi energy level of V_s-NCSP shifts to a higher position than V_s-CSP, ascribed to the formation of

This journal is © The Royal Society of Chemistry 20xx

Please do not adjust margins

Please do not adjust margins

heterointerface. On the contrary, before phosphidation, the NCS samples possess the higher Co d-band in the Fermi energy level, suggesting that S contributes to the localization of Co 3d electron orbital around the Fermi energy level.[15-17] The above analysis suggests that the H adsorption energy is in order of NCS > V_S-NCSP > V_S-CSP, yet overvalued adsorption energy becomes negative to the H desorption process. Furthermore, the differential charge density of the model (Fig. 5e-f and Fig. S20-S21) indicates that the electron is transferred between Ni-based and the Co-based moieties of V_S-NCSP, which positively affect the activity of systems due to the formation of heterointerface and P elements. These further imply the strong interface electronic interaction between Ni-based and Co-based group. Besides, the NCS samples obtain more changes relative to V_S-NCSP in the heterointerface. Hence, we presume that the NCS sample does not easily detach H atoms, and the P anion can balance the H adsorption/desorption energy. The Gibbs free energy (ΔG_{H^*}) diagram and model on Co-site for the HER pathway are depicted in Fig. 5g and inset images of Fig. 5g. For the NCS, the ΔG_{H^*} on Co-site is -0.04 eV, meaning the H adsorption is too tight due to the negative ΔG_{H^*} value. The ΔG_{H^*} of the V_S-NCSP is 0.01 eV, which is almost close to the optimal value (0 eV), proving the fastest HER activity. Therefore, the implantation of P anion and heterointerface weaken the H adsorption, rendering enhanced HER process. As for the V_S-CSP, the ΔG_{H^*} on Co-site is 0.13 eV, which is detrimental to the HER. More necessarily, the model (Fig. S22-S24) and ΔG_{H^*} (Fig. S25, Fig. 5e) of different H adsorption sites, such as Ni, S and P sites, are calculated by DFT for V_S-NCSP, NCS and V_S-CSP. These results confirm that the optimum H adsorption site is Co-site for all catalysts based on the value of ΔG_{H^*} (V_S-NCSP: Ni sites (0.32 eV); S sites (0.26 eV); P sites (-0.08 eV). NCS: Ni sites (0.29 eV); Co sites (-0.04 eV); S sites (0.12 eV). V_S-CSP: Co sites (0.13 eV); S sites (0.31 eV); P sites (-0.23 eV)). Also, the V_S-NCSP with P anion and heterointerface gains the ΔG_{H^*} nearest to 0 eV, which matches the experimental conclusion well. On the one hand, the heterogeneous interface can control charge moving between $Ni_3S_xP_y$ and $Co_3S_xP_y$, which stimulates robust electronic interaction and further boosts the activity. On the other hand, the P anion lowers the H adsorption energy of sulfides, thereby balancing the energy of H adsorption and desorption. Therefore, the combined advantages ensure the catalyst with admirable performance for the promising HER application.

Conclusions

In summary, cross-linked porous V_S-NCSP-X/NF heterojunction with enriched S defects is constructed *via* facile dipping and hydrothermal methods, and demonstrated as an all-round HER catalyst in the universal pH range. The well-defined electrocatalysts provide a unique heterointerface, which excite controllable charge transfer between $Ni_3S_xP_y$ and $Co_3S_xP_y$ according to the DFT calculations. The introduction of P elements breaks the limitations of sulfides with high adsorption energy and obtains numerous S defects, which is conducive to the release of hydrogen atoms, gaining an optimum ΔG_{H^*} (0.01 eV). Simultaneously, P elements provide a protective layer to enhance structure stability during HER process in a wide pH range. Besides, the unique structure possesses a fast conductive network, rendering favored charge/mass transport. Thus, the as-developed material gains superior HER properties (η_{-10} = 56 mV, Tafel slopes: 74 mV dec^{-1} in 1 M KOH; η_{-10} = 69 mV, Tafel slopes: 94 mV dec^{-1} in 0.5 M H_2SO_4; η_{-10} = 90 mV, Tafel slopes: 118 mV dec^{-1} in 1.0 M PBS). This work delivers a new way to regulate electron movement and stabilize material structure as well as balance H adsorption-desorption energy of S-based catalysts to achieve remarkable electrocatalysis, which also enlightens the material design in the related energy storage and conversion area.

Author Contributions

Dawei Chu: Conceptualization, Roles/Writing - original draft, Data curation, Software, Formal analysis, Methodology, Investigation, Validation. **Xiaoling Wei**: Conceptualization, Writing - review & editing, Formal analysis, Validation. **Xiumei Song**: Conceptualization, Writing - review & editing, Formal analysis, Validation. **Zhen Zhang**: Conceptualization, Writing - review & editing, Formal analysis, Validation. **Lichao Tan**: Conceptualization, Writing - review & editing, Resources, Funding acquisition. **Huiyuan Ma**: Conceptualization, Writing - review & editing, Resources, Funding acquisition. **Haijun Pang**: Conceptualization, Validation, Resources. **Xin Wang**: Methodology, Software. **Zhongwei Chen**: Conceptualization, Writing - review & editing, Resources, Funding acquisition.

Conflicts of interest

There are no conflicts to declare.

Acknowledgements

This work was financially supported by Major Research Plan National Natural Science Foundation of China (92061102), the Natural Science Foundation of Heilongjiang Province (LH2019B009) and the Fundamental Research Foundation for Universities of Heilongjiang Province (LGYC2018JC009, 2019-KYYWF-0219), the Postdoctoral Scientific Research Developmental Fund of Heilongjiang Province (LBH-Q20023), Natural Science Foundation of Guangdong Province (2214050007080), Natural Sciences and Engineering Research Council of Canada, University of Waterloo, and Waterloo Institute for Nanotechnology. The authors also acknowledge the XPS characterizations at the Vacuum Interconnected Nanotech Workstation (Nano-X), Suzhou Institute of Nano-Tech and Nano-Bionics, Chinese Academy of Sciences. Dawei Chu is grateful to the China Scholarship Council for the financial support (No. 202008230253).

References

1 D. Song, J. Sun, L. Sun, S. Zhai, G.W. Ho, H. Wu, W.Q. Deng, *Adv. Energy Mater.*, 2021, **11**, 2100358.
2 M.R. Gao, J.X. Liang, Y.R. Zheng, Y.F. Xu, J. Jiang, Q. Gao, J. Li, S.H. Yu, *Nat. Commun.*, 2015, **6**, 5982.

Please do not adjust margins

Please do not adjust margins

3 M.A.R. Anjum, M.S. Okyay, M. Kim, M.H. Lee, N. Park, J.S. Lee, *Nano Energy*, 2018, **53**, 286-295.
4 S. Shen, Z. Wang, Z. Lin, K. Song, Q. Zhang, F. Meng, L. Gu, W. Zhong, *Adv. Mater.*, 2022, **34**, 2110631-2110639.
5 X. Wang, Y. Fei, J. Chen, Y. Pan, W. Yuan, L.Y. Zhang, C.X. Guo, C.M. Li, *Small*, 2022, **18**, 2103866-2103882.
6 K.L. Zhou, Z. Wang, C.B. Han, X. Ke, C. Wang, Y. Jin, Q. Zhang, J. Liu, H. Wang, H. Yan, *Nat. Commun.*, 2021, **12**, 3783.
7 P. Kuang, Y. Wang, B. Zhu, F. Xia, C.W. Tung, J. Wu, H.M. Chen, J. Yu, *Adv. Mater.*, 2021, **33**, 2008599.
8 J. Chen, G. Qian, H. Zhang, S. Feng, Y. Mo, L. Luo, S. Yin, *Adv. Funct. Mater.*, 2021, **32**, 2107597.
9 W. Zhang, B. Huang, K. Wang, W. Yang, F. Lv, N. Li, Y. Chao, P. Zhou, Y. Yang, Y. Li, J. Zhou, W. Zhang, Y. Du, D. Su, S. Guo, *Adv. Energy Mater.*, 2020, 11, 2003192.
10 S. Anantharaj, S.R. Ede, K. Sakthikumar, K. Karthick, S. Mishra, S. Kundu, *ACS Catal.*, 2016, **6**, 8069-8097.
11 F. Zheng, W. Zhang, X. Zhang, Y. Zhang, W. Chen, *Adv. Funct. Mater.*, 2021, **31**, 2103318.
12 Q. Liang, L. Zhong, C. Du, Y. Luo, J. Zhao, Y. Zheng, J. Xu, J. Ma, C. Liu, S. Li, Q. Yan, *ACS Nano*, 2019, **13**, 7975-7984.
13 L. Song, Q. Wang, X. Ye, F. Yang, L. Wang, Y. Wu, F. Xu, Y. Wang, *ACS Mater. Lett.*, 2021, **3**, 1016-1024.
14 J. Jin, J. Yin, H. Liu, B. Huang, Y. Hu, H. Zhang, M. Sun, Y. Peng, P. Xi, C.H. Yan, *Angew. Chem. Int. Ed.*, 2021, **60**, 14117-14123.
15 R. Boppella, J. Park, H. Lee, G. Jang, J. Moon, *Small Methods*, 2020, **4**, 2000043.
16 H.J. Song, H. Yoon, B. Ju, G.-H. Lee, D.-W. Kim, *Adv. Energy Mater.*, 2018, **8**, 1802319.
17 V.Q. Bui, A. Kumar, H.T.D. Bui, J. Lee, Y. Hwang, H.M. Le, Y. Kawazoe, H. Lee, *Chem. Mater.,* 2020, **32**, 9591-9601.
18 J. Sun, H. Xue, N. Guo, T. Song, Y.R. Hao, J. Sun, J. Zhang, Q. Wang, *Angew. Chem. Int. Ed.*, 2021, **60**, 19435-19441.
19 P. Xue, C. Guo, L. Li, H. Li, D. Luo, L. Tan, Z. Chen, Adv. Mater. 34 (2022), 2110047.
20 D. Ji, L. Fan, L. Tao, Y. Sun, M. Li, G. Yang, T.Q. Tran, S. Ramakrishna, S. Guo, *Angew. Chem. Int. Ed.*, 2019, 58, 13840-13844.
21 X. Li, Q. Hu, H. Wang, M. Chen, X. Hao, Y. Ma, J. Liu, K. Tang, A. Abudula, G. Guan, *Appl. Catal. B.*, 2021, **292**, 120172.
22 D. Chu, X. Zhao, B. Xiao, A. Libanori, Y. Zhou, L. Tan, H. Ma, H. Pang, X. Wang, Y. Jiang, J. Chen, *Chem. Eur. J.*, 2021, **27**, 8337-8343.
23 P. Gao, Y. Zeng, P. Tang, Z. Wang, J. Yang, A. Hu, J. Liu, *Adv. Funct. Mater.*, 2021, **32**, 2108644.
24 P. Wang, Y. Luo, G. Zhang, M. Wu, Z. Chen, S. Sun, Z. Shi, *Small*, 2022, **18**, 2105803.
25 L. An, Z. Zhang, J. Feng, F. Lv, Y. Li, R. Wang, M. Lu, R.B. Gupta, P. Xi, S. Zhang, *J. Am. Chem. Soc.*, 2018, **140**, 17624-17631.
26 M. Yan, Z. Zhao, P. Cui, K. Mao, C. Chen, X. Wang, Q. Wu, H. Yang, L. Yang, Z. Hu, *Nano Res.*, 2021, **14**, 4220-4226.
27 Z. Cai, Y. Bi, E. Hu, W. Liu, N. Dwarica, Y. Tian, X. Li, Y. Kuang, Y. Li, X.Q. Yang, H. Wang, X. Sun, *Adv. Energy Mater.*, 2017, **8**, 1701694.
28 X. Xiong, C. Mao, Z. Yang, Q. Zhang, G.I.N. Waterhouse, L. Gu, T. Zhang, *Adv. Energy Mater.*, 2020, **10**, 2001928.
29 X. Zhang, S. Deng, Y. Zeng, M. Yu, Y. Zhong, X. Xia, Y. Tong, X. Lu, *Adv. Funct. Mater.*, 2018, **28**, 1805618.
30 K. Zheng, Y. Zeng, S. Liu, C. Zeng, Y. Tong, Z. Zheng, T. Zhu, X. Lu, *Energy Storage Mater.*, 2019, **22**, 410-417.
31 S. Liu, Y. Yin, D. Ni, K.S. Hui, M. Ma, S. Park, K.N. Hui, C.-Y. Ouyang, S.C. Jun, *Energy Storage Mater.*, 2019, **22**, 384-396.
32 X. Liu, S. Ding, L. Ye, Y. Du, L. Zhao, Y. Zhu, *Chem. Eng. J.*, 2020, **399**, 125789.
33 C. Tang, Q. Zhang, J. Wu, H. Chen, L. Chen, C.M. Li, *ACS Sus. Chem. Eng.*, 2018, **6**, 15618-15623.
34 H. Fei, T. Guo, Y. Xin, L. Wang, R. Liu, D. Wang, F. Liu, Z. Wu, *Appl. Catal. B.*, 2022, **300**, 120733.
35 X. Zhang, C. Shang, E.M. Akinoglu, X. Wang, G. Zhou, *Adv. Sci.*, 2020, **7**, 2002037.
36 H. Su, S. Song, S. Li, Y. Gao, L. Ge, W. Song, T. Ma, J. Liu, *Appl. Catal. B.*, 2021, **293**, 120225.
37 Q. Wu, A. Dong, C. Yang, L. Ye, L. Zhao, Q. Jiang, *Chem. Eng. J.*, **413**, 127482.
38 P. Thangasamy, S. Oh, S. Nam, H. Randriamahazaka, I.K. Oh, *Small*, 2020, **16**, 2001665.
39 D. Guo, J. Wang, L. Zhang, X. Chen, Z. Wan, B. Xi, *Small*, 2020, **16**, 2002432.
40 O. Peng, R. Shi, J. Wang, X. Zhang, J. Miao, L. Zhang, Y. Fu, P. Madhusudan, K. Liu, A. Amini, C. Cheng, *Mater. Today Energy*, 2020, **18**, 100513.
41 L. Zhang, Y. Zheng, J. Wang, Y. Geng, B. Zhang, J. He, J. Xue, T. Frauenheim, M. Li, *Small*, 2021, **17**, 2006730.
42 R. Li, B. Hu, T. Yu, Z. Shao, Y. Wang, S. Song, *Small Methods*, 2021, **5**, 2100246.
43 Y. Yang, H. Yao, Z. Yu, S. M. Islam, H. He, M. Yuan, Y. Yue, K. Xu, W. Hao, G. Sun, H. Li, S. Ma, P. Zapol, M. G. Kanatzidis, *J. Am. Chem. Soc.*, 2019, **141**, 10417.
44 L. Li, C. Sun, B. Shang, Q. Li, J. Lei, N. Li, F. Pan, *J. Mater. Chem. A.*, 2019, **7**, 18003-18011.
45 A. Sivanantham, P. Ganesan, S. Shanmugam, *Adv. Funct. Mater.*, 2016, **26**, 4661-4672.
46 H. Liu, X. Ma, Y. Rao, Y. Liu, J. Liu, L. Wang, M. Wu, *ACS Appl. Mater. Interfaces.*, 2018, **10**, 10890-10897.
47 F. Du, L. Shi, Y. Zhang, T. Li, J. Wang, G. Wen, A. Alsaedi, T. Hayat, Y. Zhou, Z. Zou, *Appl.Catal. B.*, 2019, **253**, 246-252.
48 T. Kou, T. Smart, B. Yao, I. Chen, D. Thota, Y. Ping, Y. Li, *Adv. Energy Mater.*, 2018, **8**, 1703538.
49 T. Zhu, L. Zhu, J. Wang, G.W. Ho, *J. Mater. Chem. A.*, 2016, **4**, 13916-13922.
50 J. Liu, J. Wang, B. Zhang, Y. Ruan, L. Lv, X. Ji, K. Xu, L. Miao, J. Jiang, *ACS Appl. Mater. Interfaces*, 2017, **9**, 15364-15372.
51 X. Xiao, L. Tao, M. Li, X. Lv, D. Huang, X. Jiang, H. Pan, M. Wang, Y. Shen, *Chem. Sci.*, 2018, **9**, 1970-1975.
52 K. Ao, D. Li, Y. Yao, P. Lv, Y. Cai, Q. Wei, *Electrochim. Acta*, 2018, **264**, 157-165.
53 Y. Li, B. Zhang, W. Wang, X. Shi, J. Zhang, R. Wang, B. He, Q. Wang, J. Jiang, Y. Gong, H. Wang, *Chem. Eng. J.*, 2021, **405**, 126981.
54 Y. Wu, Y. Wang, Z. Wang, X. Li, *J. Mater. Chem. A.*, 2021, **9**, 23574-23581.
55 J. Zhang, Z. Zhang, Y. Ji, J. Yang, K. Fan, X. Ma, C. Wang, R. Shu, Y. Chen, *Appl. Catal. B.*, 2021, **282**, 119609.
56 T.L.L. Doan, D.C. Nguyen, S. Prabhakaran, D.H. Kim, D.T. Tran, N.H. Kim, J.H. Lee, *Adv. Funct. Mater.*, 2021, **31**, 2100233.
57 Y. Pan, K. Sun, Y. Lin, X. Cao, Y. Cheng, S. Liu, L. Zeng, W.-C. Cheong, D. Zhao, K. Wu, Z. Liu, Y. Liu, D. Wang, Q. Peng, C. Chen, Y. Li, *Nano Energy*, 2019, **56**, 411-419.
58 Z.F. Huang, J. Song, K. Li, M. Tahir, Y.T. Wang, L. Pan, L. Wang, X. Zhang, J.J. Zou, *J. Am. Chem. Soc.*, 2016, **138**, 1359-1365.
59 Z. Chen, R. Wu, Y. Liu, Y. Ha, Y. Guo, D. Sun, M. Liu, F. Fang, *Adv. Mater.*, 2018, **30**, 1802011.
60 Y. Li, S. Niu, D. Rakov, Y. Wang, M. Caban-Acevedo, S. Zheng, B. Song, P. Xu, *Nanoscale*, 2018, **10**, 7291-7297.
61 P. Ji, H. Jin, H. Xia, X. Luo, J. Zhu, Z. Pu, S. Mu, *ACS Appl. Mater. Interfaces*, 2020, **12**, 727-733.
62 Z. Pu, C. Zhang, I.S. Amiinu, W. Li, L. Wu, S. Mu, *ACS Appl. Mater. Interfaces*, 2017, **9**, 16187-16193.
63 X. Liu, B. Wen, R. Guo, J. Meng, Z. Liu, W. Yang, C. Niu, Q. Li, L. Mai, *Nanoscale*, 2018, **10**, 9856-9861.
64 H. Xue, A. Meng, H. Zhang, Y. Lin, Z. Li, C. Wang, *Nano Res.*, 2021, **14**, 4173-4181.
65 T. Liu, X. Ma, D. Liu, S. Hao, G. Du, Y. Ma, A.M. Asiri, X. Sun, L. Chen, *ACS Catal.*, 2016, **7**, 98-102.
66 Y. Sun, Z. Xue, Q. Liu, Y. Jia, Y. Li, K. Liu, Y. Lin, M. Liu, G. Li, C.Y. Su, *Nat. Commun.*, 2021, **12**, 1369.

This journal is © The Royal Society of Chemistry 20xx

Please do not adjust margins